Rate dependence of grain boundary sliding via time-scaling atomistic simulations

Farah Hammami and Yashashree Kulkarni

Citation: Journal of Applied Physics **121**, 085303 (2017); doi: 10.1063/1.4977105
View online: http://dx.doi.org/10.1063/1.4977105
View Table of Contents: http://aip.scitation.org/toc/jap/121/8
Published by the American Institute of Physics

Rate dependence of grain boundary sliding via time-scaling atomistic simulations

Farah Hammami and Yashashree Kulkarni[a)]
Department of Mechanical Engineering, University of Houston, Houston, Texas 77204, USA

(Received 21 December 2016; accepted 9 February 2017; published online 27 February 2017)

Approaching experimentally relevant strain rates has been a long-standing challenge for molecular dynamics method which captures phenomena typically on the scale of nanoseconds or at strain rates of 10^7 s^{-1} and higher. Here, we use grain boundary sliding in nanostructures as a paradigmatic problem to investigate rate dependence using atomistic simulations. We employ a combination of time-scaling computational approaches, including the autonomous basin climbing method, the nudged elastic band method, and kinetic Monte Carlo, to access strain rates ranging from 0.5 s^{-1} to 10^7 s^{-1}. Combined with a standard linear solid model for viscoelastic behavior, our simulations reveal that grain boundary sliding exhibits noticeable rate dependence only below strain rates on the order of 10 s^{-1} but is rate independent and consistent with molecular dynamics at higher strain rates. *Published by AIP Publishing*. [http://dx.doi.org/10.1063/1.4977105]

I. INTRODUCTION

Grain boundaries (GBs) play an important role in determining the mechanical properties of polycrystalline materials such as strength, toughness, and creep.[1] This becomes even more accentuated as the microstructural dimensions reach the nanoscale. Owing to the high density of interfaces, the mechanical response of nanocrystalline materials is primarily governed by grain boundary mediated processes such as sliding, migration, and interaction of dislocations with grain boundaries (see Ref. 2 for a review). In particular, one of the key atomistic mechanisms governing creep in polycrystalline materials is grain boundary sliding and diffusion.[3–7] Hence, although grain boundary sliding and its role in creep have been actively studied over the past decades providing vital insights, renewed efforts are being invested in experiments and simulations to provide atomistic insights into grain boundary sliding in nanostructures.[8–15] While conventional molecular dynamics (MD) methods have played an important role in shaping our understanding of deformation mechanisms in nanostructured materials, they have been severely limited to timescales of nanoseconds or strain rates of 10^7 s^{-1} and higher. This bottleneck stems from the fact that a typical MD timestep is about a femtosecond in order to capture the thermal vibrations of the atoms. This has rendered them incapable of furnishing physical insights with atomistic fidelity into time-dependent deformation such as creep, and the associated grain boundary sliding and diffusion, which typically occur on the timescale of seconds and beyond, even years.

Recently, a novel energy landscape sampling approach known as the autonomous basin climbing (ABC) method was developed by Yip and coworkers,[16,17] to enable the study of time-dependent phenomena while maintaining atomistic resolution. Over the years, the ABC approach and the methods based on these ideas have shown great promise in modeling phenomena governed by rare events and slow processes such as creep, grain boundary sliding, diffusion, and strain rate sensitivity, problems that have so far been beyond the scope of conventional atomistic methods.[14,16–25] Gouissem *et al.*[14] employed the ABC method to obtain, from atomistics, a constitutive law for grain boundary sliding and provide fresh insights into the largely phenomenological theories for grain boundary sliding. They compared their results with the MD simulations of Qi and Krajewski,[10] which showed the existence of a threshold force below which the grain boundary sliding cannot be observed. In contrast, Gouissem *et al.* revealed that the threshold was in fact negligible if the system was allowed enough time to jump from a stable state to another by reaching a time scale of milliseconds instead of only picoseconds. Fan *et al.*[21] studied the interaction of an edge dislocation with a cluster of self-interstitial atoms using a constant strain rate version of this time-scaling approach. They reported a new deformation mechanism as they reached low strain rates of 10^3 s^{-1}, which was previously unobserved via conventional MD. Yan and Sharma[25] further demonstrated the importance of time-scaling in atomistics by simulating nanopillar compression at difference strain rates. Interestingly, their work revealed that although the high strain rate behavior shows defect structures comparable to conventional MD, the slow compression leads to a liquid-like behavior, which was consistent with experiments.

In this work, we seek to elucidate the rate dependence of grain boundary sliding in nanostructures by employing the new iterative strain method, a modification of the ABC method, introduced by Fan *et al.*[21] Specifically, we investigate the effect of strain rates on grain boundary sliding in an aluminum nanopillar under shear deformation. The key steps of our time-scaling computational approach are as follows (Fig. 1): (1) ABC algorithm is used to sample the potential energy surface (PES) at a constant prescribed shear strain; (2) Nudged elastic band method (NEB) is used to refine the energy barriers between two minima furnished by ABC; (3)

a)Electronic mail: ykulkarni@uh.edu

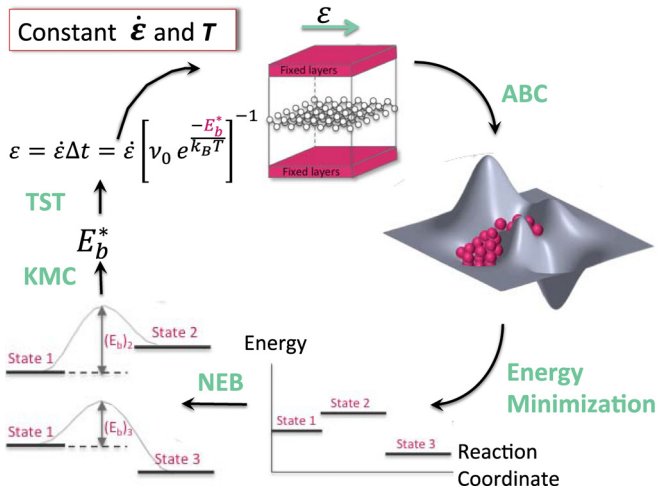

FIG. 1. Algorithm for the time-scaling atomistic method used in this study.

Kinetic Monte Carlo (KMC) is used to predict the most probable final state based on the activation barriers for various events; (4) Given a constant strain rate and temperature, the new increment of strain is calculated based on the transition state theory (TST). The details of the computational approach are provided in Sec. II.

II. SIMULATION METHODOLOGY

In this study, we use a symmetrical Σ5(310)[001] tilt GB in an Al bicrystal as a representative grain boundary in a face-centered-cubic crystal structure (Fig. 2). The tilt axis of this GB is along the [001] direction which is aligned with the z axis of our specimen. The symmetrical tilt GB can be constructed by taking two face-centered-cubic (fcc) grains of the same material and crystallographic orientation and rotating them around the tilt axis such that the upper grain is rotated by $-\frac{\theta}{2}$ and the lower is rotated by $\frac{\theta}{2}$. The mirror symmetry of the two grains can then be viewed with respect to the tilt axis.[9] This GB corresponds to a tilt angle θ of 36.87° and is considered to be a high angle GB.

All simulations are performed in LAMMPS.[26] The bicrystal is created at 0 K using the code developed by Tschopp and McDowell.[27] The atomistic interactions are modeled using the embedded-atom (EAM) interatomic

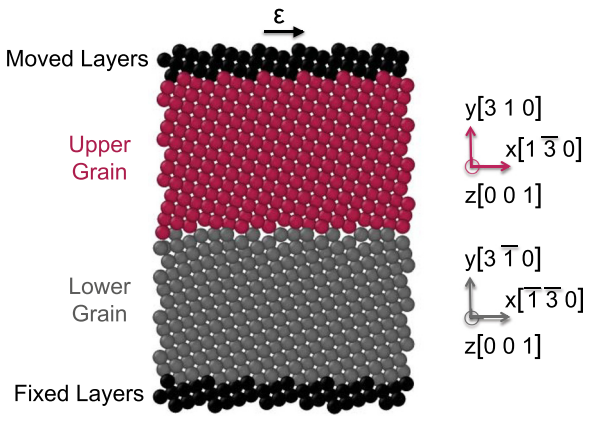

FIG. 2. Cross-section showing the atomistic structure of the bicrystalline nanopillar containing a Σ5(310)[001] GB.

potential developed by Liu *et al.*[28] for Al. The initial supercell is periodic in all directions and consists of 57 120 atoms. The potential energy is first minimized through the conjugate gradient method, and then, the system is equilibrated at 300 K for 50 ps under the NPT thermodynamic ensemble. The actual non-periodic bicrystal used in our study is obtained by cutting it out of the supercell in order to study the grain boundary mediated deformation in a nanostructure. The final dimensions of this structure are 40 Å × 58 Å × 38 Å. The specimen consists of 5616 atoms.

The various components of the time-scaling algorithm used in our study are illustrated schematically in Fig. 1. The ABC method is an activation-relaxation technique for sampling the potential energy landscape starting with the system in an initial local minimum. This is achieved by applying a penalty function to the potential energy of a system of particles with or without external loading (activation) followed by static energy minimization (relaxation). The 3N-dimensional penalty function is assumed to be Gaussian and expressed as

$$\Phi_p^k(r) = \omega \exp\left[-\frac{(r - r_{min}^k)}{2\sigma^2}\right], \tag{1}$$

where ω and σ are the parameters for the Gaussian distribution: ω controls the height and σ refers to the width. r_{min}^k is the position at the minimum configuration and the applied penalty iteration k. Repeating this process eventually pushes the system out of its initial well into another neighboring local minimum. In our study, the ABC method is applied under a prescribed strain (which is zero in the initial run).

Although ABC is an efficient and reliable method for capturing energy barriers and atomistic configurations at the identified minima without knowing the final states *a priori*, the penalty functions affect the accuracy of the saddle points between consecutive minima and it is now known that the activation barriers tend to be overestimated.[16,25] To overcome this issues, we enrich the model by employing the NEB method[29] to extract more accurate minimum energy pathways and transition state configurations between the initial state and the different possible final states collected through ABC. Based on a matrix of these different energy barriers, KMC[30] is employed to predict the most probable final state the system is likely to move to from an initial minimum. KMC invokes the TST to determine the rate constant associated with each barrier crossing expressed as

$$k_{ij} \propto \exp\left[-\frac{\Delta E}{k_B T}\right], \tag{2}$$

where k_{ij} is the rate constant for one single barrier crossing event from minimum i to minimum j, ΔE is the barrier energy calculated from NEB, k_B is the Boltzmann constant, and T is the temperature. In KMC simulations, the probability of each transition event is defined as the rate constant of this event divided by the summation of the rate constants for all possible transitions from the current state. Thus, KMC method allows us to predict the most probable path that the system is going to take during microstructural evolution by

determining the most probable jump from the current state to all possible final states collected by ABC (initial–final1–final2–final3… finaln) instead of limiting the choice to two collected stable states from ABC (initial–final) (Fig. 1). In order to account even for the low probability events, a random number in the range of (0–1) is generated each time, and one of the events acquiring a probability higher than this number is selected.

The last key step in the algorithm is the modified version of ABC method for constant strain rate proposed by Fan *et al.*[21] Once a possible transition event is selected through KMC, the harmonic approximation of the TST is invoked to determine the transition time Δt for the event as

$$\Delta t = \left[\nu_0 \exp\left[-\frac{\Delta E}{k_B T}\right]\right]^{-1}, \tag{3}$$

where ν_0 is the jump frequency taken to be about 10^{13} s^{-1} and ΔE is the energy barrier between two states calculated from NEB as before. Then, the new strain to be applied in the subsequent ABC run is estimated by using the relation $\epsilon = \dot{\epsilon}\Delta t$ for a given constant temperature and strain rate $\dot{\epsilon}$. We emphasize that TST enables us to account for the effect of the temperature which is not considered during the activation-relaxation step of ABC as it simply maps the PES through molecular statics. In the present study, we implement three shear simulations at 300 K under strain rates ranging from those comparable to MD to those beyond the scope of MD. The results are discussed in the following section.

III. RESULTS

Using the algorithm outlined above, we perform shear simulations on the bicrystal shown in Fig. 2 at three different strain rates, specifically, $0.5\,s^{-1}$, $10^3 s^{-1}$, and $10^7 s^{-1}$. For the sake of direct comparison, MD simulation is also performed on the same structure initially equilibrated at 300 K, but deformed at a temperature close to zero under a strain rate of $10^7 s^{-1}$.

Fig. 3 shows the stress versus strain plot for different strain rates using the time-scaling approach and MD. Overall, we observe two different trends: the $10^7 s^{-1}$ and $10^3 s^{-1}$ stress-strain curves from ABC show a behavior that is consistent with MD, whereas the 0.5 s^{-1} strain rate results are distinct. Nevertheless, the deformation mechanism under all the different strain rates investigated using both approaches is primarily grain boundary sliding as shown in Fig. 4. The method used to identify the GB deformation mechanism as sliding is described below. We also performed MD simulations on the same grain boundary with periodic boundary conditions (to simulate an infinitely large specimen), and we found that the deformation mechanism under shear was still GB sliding. Since the deformation mechanism remains the same, we note that it enables us to study the rate dependence of a specific mechanism.

The agreement between the time-scaling approach and MD results for the $10^7 s^{-1}$ strain rate is expected and serves to validate our time-scaling simulations. For the $10^7 s^{-1}$ strain rate, the system yields at 1.2 GPa which is only about 7.7%

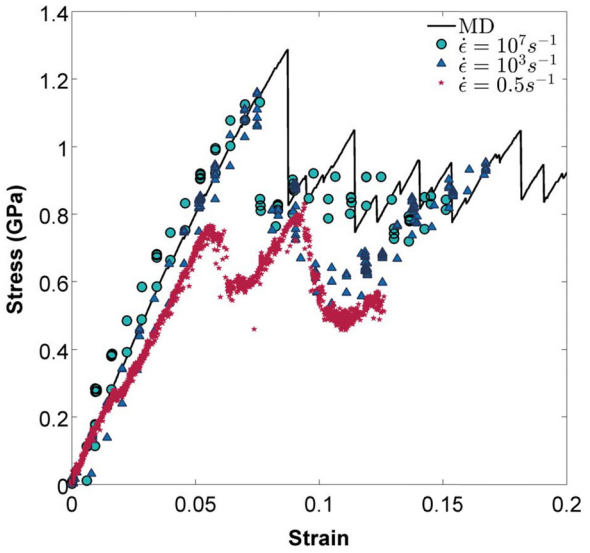

FIG. 3. Stress versus strain plots for different strain rates using the time-scaling approach and molecular dynamics.

lower than MD. The elastic modulus calculated from both methods is identical. More importantly, the post-yield saw tooth behavior in both cases is also similar. Interestingly, the overall stress-strain response and the yield stress, at a much lower strain rate of $10^3 s^{-1}$, are almost similar to the $10^7 s^{-1}$ case, although it shows some minor differences in the plastic behavior. Specifically, the stress in the $10^3 s^{-1}$ strain rate case shows a more drastic drop after yield than the $10^7 s^{-1}$ case. In order to quantify the GB sliding, we track two atoms, one in the upper grain and the other in the lower grain. Both atoms are chosen to be in the center of the nanopillar and at about 5 Å from the grain boundary. The positions in the x-direction of these atoms are recorded for every reaction coordinate. The GB sliding is defined as the difference between the x-coordinates of the tracked atoms at every reaction coordinate. Fig. 5 displays the sliding as a function of the strain for the different cases.

Fig. 5 reveals that the sliding versus strain response for the $10^3 s^{-1}$ and $10^7 s^{-1}$ high strain rate ABC is in agreement

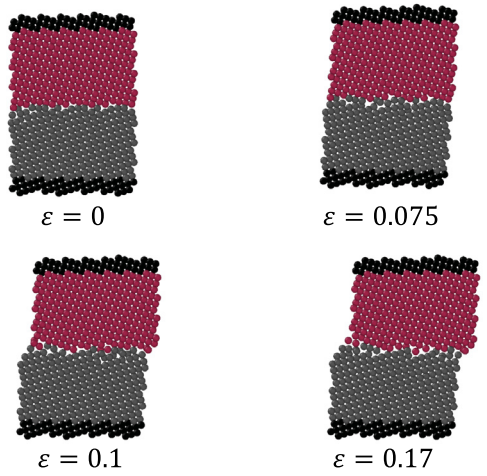

FIG. 4. Atomistic structures showing grain boundary sliding at different strains for the strain rate of $10^3 s^{-1}$.

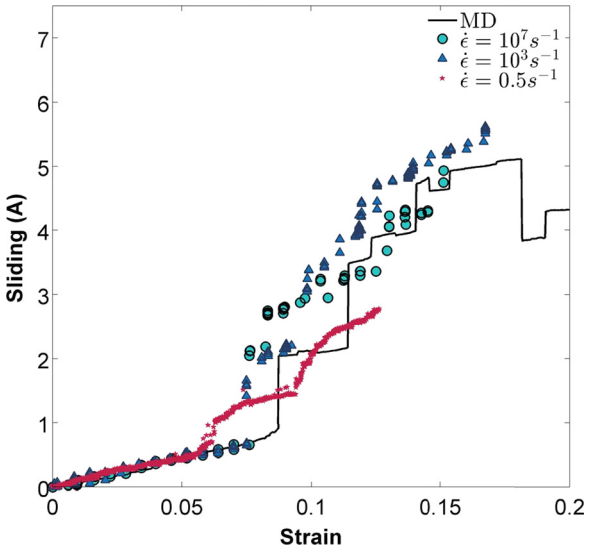

FIG. 5. GB sliding versus strain plots for different strain rates using ABC and MD.

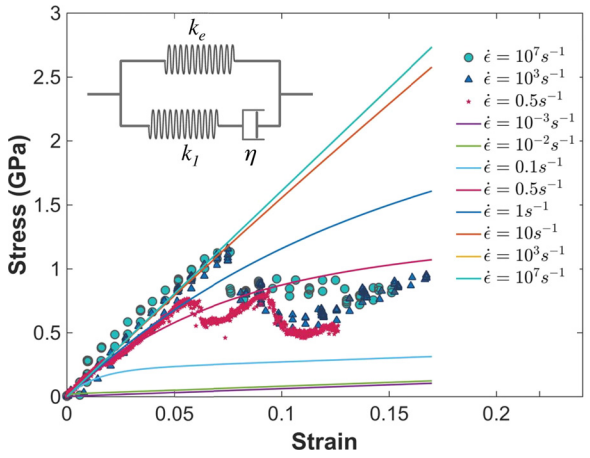

FIG. 6. Stress-strain curves for different strain rates predicted by fitting the standard linear solid spring-dashpot model to simulation data. The discrete points indicate simulation data, while solid lines represent the curves obtained from the spring-dashpot model.

with the MD results. In addition, comparing Figs. 3 and 5, we note that the larger drops in stress correspond to relatively greater GB sliding in the case of the $10^3 s^{-1}$ strain rate than the $10^7 s^{-1}$ case.

In contrast, the stress-strain curve (Fig. 3) for the low strain rate of 0.5 s^{-1} reveals a significantly lower yield stress. Although the elastic modulus appears to be rate independent, the yield occurs at a much lower stress of 0.8 GPa, which is about 38% lower than the yield stress at MD strain rate. Early yielding indicates that a different deformation mechanism than the high strain rate might be at play at the low strain rate. Thus, we consider the assessment of all possible mechanisms—GB sliding, GB migration, or GB rotation—that could have occurred albeit in small magnitude. We use several processing techniques to quantify all these possible mechanisms. In order to estimate the migration, we track the same atoms that we use for estimating the sliding but in the normal (y) direction. We do not notice any measurable GB migration. For GB rotation, we follow the approach by Cheng *et al.*[13] and do not observe any occurrence of GB rotation. Finally, we quantify the GB sliding using the same technique described earlier and indeed observe GB sliding with jumps in sliding corresponding to drops in stress. Thus, we conclude that the deformation mechanism at low strain rates is basically GB sliding, but the increments are smaller and occur at stresses lower than the high strain rate cases (Figs. 3 and 5).

IV. DISCUSSION

To quantify the rate dependence revealed in our simulations, we note that mechanics of grain boundary sliding can be understood as a viscous response.[1,3,5] To this end, we use the spring dashpot model for a standard linear solid as shown in the inset of Fig. 6. Here, k_e denotes the stiffness of the spring that corresponds to the elastic component, η and k_1 denote, respectively, the viscosity and the stiffness of the spring in the Maxwell arm that corresponds to the viscoelastic component. Then, for constant strain rate, R, the stress-strain relation is given by

$$\sigma = k_e \varepsilon + R\eta\left[1 - \exp^{-\frac{k_1}{R\eta}\varepsilon}\right]. \tag{4}$$

The simulation results for the three strain rates are fitted to this equation to obtain estimates for the three material parameters. Given $\frac{k_1}{\eta R}$ for a particular grain boundary, there should be a certain strain rate R above which the behavior or sliding will be strain rate independent. Using the least square method for fitting the simulation data yields $k_e = 0.6$ GPa, $k_1 = 15.5$ GPa, and $\eta = 2.1$ GPa-sec. Taylor's expansion of the exponential term shows that when the strain is much smaller than $\frac{\eta R}{k_1}$, the response is rate independent and we obtain the Hooke's law

$$\sigma = (k_e + k_1)\varepsilon. \tag{5}$$

Using the parameter values extracted above, the factor $\frac{\eta R}{k_1}$ is estimated to be about $0.15R$. Considering that the applied strains reach up to 0.2 (20% strain), the model predicts that grain boundary sliding should become rate independent at strain rates of around 10 or higher. This is an interesting revelation and also consistent with our simulations that indicate strain rate independence at $10^3 s^{-1}$ and $10^7 s^{-1}$ strain rates. Furthermore, our simulations indicate that the shear modulus is rate independent. Based on the above expression, the shear modulus is given by $k_e + k_1$ which is about 16 GPa and is consistent with the modulus obtained for Al directly from MD simulation for the given interatomic potential.

Fig. 6 shows the stress-strain curves for different strain rates predicted by fitting the standard linear spring-dashpot model to simulation data. As estimated above, we observe that the grain boundary sliding indeed exhibits noticeable rate dependence below strain rates on the order of 10 s^{-1} and is rate independent and consistent with molecular dynamics at higher strain rates. We would like to mention that since we assume a linear spring dashpot model, it captures the rate independent elastic part at higher strain rates but does not

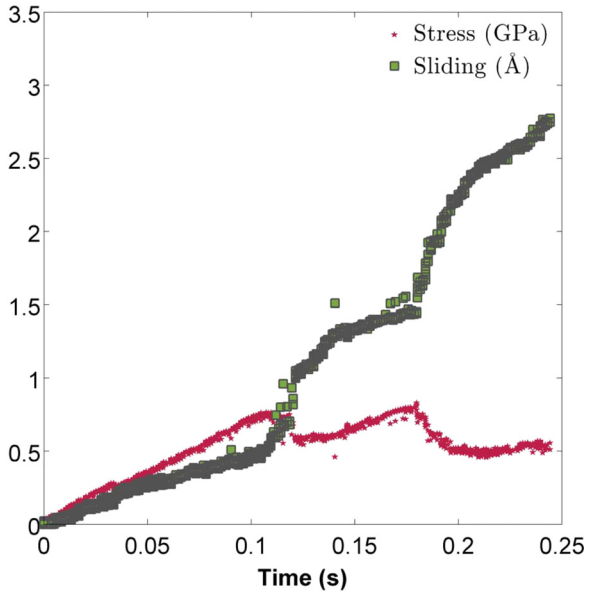

FIG. 7. Stress and GB sliding versus time for the low strain rate of $\dot{\epsilon} = 0.5\,s^{-1}$.

capture the rate independent plasticity and the yield stress. The model can be enriched further to predict the yielding even at high strain rates by using a spring with a nonlinear power-law behavior. Nevertheless, the present model suffices to make a quantitative prediction of when the deformation mechanism becomes rate independent which is the focus of this paper.

Finally, we wish to note that although the stress versus strain and sliding versus strain curves are insightful, the importance of time-scaling approaches is further emphasized by plotting the stress and sliding versus time. As shown in Fig. 7, the time-scaling method is able to capture GB sliding that occurs on the order of seconds when the strain rate is $0.5\ s^{-1}$. Accessing these time scales while maintaining atomistic resolution is beyond the scope of molecular dynamics by several orders of magnitude.

V. CONCLUSION

In this work, we investigate the strain rate dependence of grain boundary sliding in nanostructures by way of recently developed time-scaling atomistic approaches. The shearing of a nanopillar with a high angle grain boundary is used as a representative problem. We employ a combination of techniques including the autonomous basin climbing method, the nudged elastic band method, and kinetic Monte Carlo, to sample the potential energy landscape of the system and capture its behavior under strain rates ranging from $0.5\ s^{-1}$ to $10^7\ s^{-1}$. Combined with the standard linear solid model for viscoelastic behavior, our study furnishes quantitative predictions about the rate sensitivity of grain boundary sliding. As the deformation mechanism for this grain boundary structure remains the same at all strain rates, it is revealed that sliding becomes rate independent beyond strain rates of the order of $10\ s^{-1}$ and hence consistent with molecular dynamics. The ramifications of this conclusion are two-fold. Since it shows the validity of molecular dynamics results over several orders of magnitude, it offers avenues to bridge the gap between experiments and molecular dynamics simulations, specifically in investigating grain boundary sliding and atomistic origins of creep. Furthermore, taken together with other studies, it provides evidence for the quantitative insights inaccessible to conventional atomistic methods that can be gleaned from time-scaling computational approaches.

ACKNOWLEDGMENTS

The authors would like to acknowledge the support from the U.S. National Science Foundation under grants CMMI-1129041 and DMR-1508484. The simulations were performed on the supercomputing facility hosted by the Research Computing Center at University of Houston. The authors would also like to thank Professor Pradeep Sharma and Dr. Xin Yan for insightful discussions.

[1]A. P. Sutton and R. W. Balluffi, *Interfaces in Crystalline Materials* (Oxford, 1995).
[2]M. Dao, L. Lu, R. J. Asaro, J. T. M. Hosson, and E. Ma, Acta Mater. **55**, 4041 (2007).
[3]H. Riedel, *Fracture at High Temperatures* (Springer-Verlag, 1987).
[4]R. Raj and M. F. Ashby, Metall. Trans. **2**, 1113 (1971).
[5]E. W. Hart, ASME J. Eng. Mater. Tech. **98**, 193 (1976).
[6]I. W. Chen and A. S. Argon, Acta Metall. **27**, 749 (1979).
[7]A. Needleman and J. R. Rice, Acta Metall. **28**, 1315 (1980).
[8]H. Van Swygenhoven and P. M. Derlet, "Grain-boundary sliding in nanocrystalline fcc metals," Phys. Rev. B **64**, 224105 (2001).
[9]J. W. Cahn, Y. Mishin, and A. Suzuki, Acta Mater. **54**, 4953 (2006).
[10]Y. Qi and P. E. Krajewski, Acta Mater. **55**, 1555–1563 (2007).
[11]Y. Wei, A. F. Bower, and H. Gao, Acta Mater. **56**, 1741 (2008).
[12]Z. H. Aitken, D. Jang, C. R. Weinberger, and J. R. Greer, Small **10**, 100 (2014).
[13]K. Cheng, C. Lu, and K. Tieu, Sci. Adv. Mater. **6**(7), 1322–1329 (2014).
[14]A. Gouissem, R. Sarangi, Q. Deng, and P. Sharma, Comp. Mater. Sci. **104**, 200 (2015).
[15]S. Jiao and Y. Kulkarni, Comp. Mater. Sci. **110**, 254 (2015).
[16]A. Kushima, X. Lin, J. Eapen, J. C. Mauro, X. Qian, P. Diep, and S. Yip, J. Chem. Phy. **130**, 224504 (2009).
[17]A. Kushima, X. Lin, J. Eapen, J. C. Mauro, X. Qian, P. Diep, and S. Yip, J. Chem. Phy. **131**, 164505 (2009).
[18]T. T. Lau, A. Kushima, and S. Yip, IOP Conf. Series: Mat. Sci. Eng. **3**, 012002 (2009).
[19]T. T. Lau, A. Kushima, and S. Yip, Phys. Rev. Lett. **104**, 175501 (2010).
[20]A. Kushima, J. Easpen, J. Li, S. Yip, and T. Zhu, Eur. Phys. J. B **82**, 271 (2011).
[21]Y. Fan, Y. N. Osetskiy, S. Yip, and B. Yildiz, PNAS **110**(44), 17756–17761 (2013).
[22]P. Cao, M. Li, R. J. Heugle, H. S. Park, and X. Lin, Phys. Rev. E **86**, 016710 (2012).
[23]P. Cao, X. Lin, and H. S. Park, J. Mech. Phys. Solids **68**, 239 (2014).
[24]X. Yan, A. Gouissem, and P. Sharma, Mech. Mater. **91**, 306 (2015).
[25]X. Yan and P. Sharma, Nano Lett. **16**, 3487–3492 (2016).
[26]S. J. Plimpton, J. Comput. Phys. **117**, 1 (1995).
[27]M. A. Tschopp and D. L. McDowell, Philos. Mag. **87**, 3871–3892 (2007).
[28]X. Y. Liu, F. Ercolessi, and J. B. Adams, Modell. Simul. Mater. Sci. Eng. **12**, 665 (2004).
[29]G. Henkelman and H. Jonsson, J. Chem. Phys. **113**, 9978 (2000).
[30]A. F. Voter, "Introduction to the Kinetic Monte Carlo Method," in *Radiation Effects in Solids*, Edited by K. E. Sickafus, E. A. Kotomin, and B. P. Uberuaga (Springer, 2007).